Maize root growth, Oxygen and N availability drive formation of N_2O hotspots in soil

Pauline Sophie Rummel[1,2]*, Martin Reinhard Rasmussen[1,3], Aurélien Saghaï[4], Theresa Merl[1], Sara Hallin[4], Carsten W. Mueller[2,5], Klaus Koren[1]

[1]Aarhus University, Department of Biology, Section for Microbiology, Aarhus, Denmark

[2]University of Copenhagen, Department of Geosciences and Natural Resource Management, Geography, Copenhagen, Denmark

[3]Aarhus University, Center for Landscape Research in Sustainable Agricultural Futures, Aarhus, Denmark

[4]Swedish University of Agricultural Sciences, Department of Forest Mycology and Plant Pathology, Uppsala, Sweden

[5]Technische Universität Berlin, Institute of Ecology, Chair of Soil Science, Berlin, Germany

* correspondence: pauline.rummel@bio.au.dk

Keywords: denitrification, rhizosphere, planar optodes, microsensors, qPCR

ORCIDs
PS Rummel: https://orcid.org/0000-0001-6442-146X
MR Rasmussen: https://orcid.org/0000-0003-1511-5663
A Saghaï: https://orcid.org/0000-0002-7069-2159
T Merl: https://orcid.org/0000-0002-2999-274X
S Hallin: https://orcid.org/0000-0002-9069-9024
CW Mueller: https://orcid.org/0000-0003-4119-0544
K Koren: https://orcid.org/0000-0002-7537-3114

Summary

Plant roots modify all major controls of denitrification in soils, particularly the availability of the main substrates (NO_3^- and C_{org}), soil moisture, soil O_2 content, and root-associated microbial communities, and thus play an important role in N_2O formation. Direct in-situ measurements of N_2O concentrations in the rhizosphere are lacking, yet crucial to understanding how rhizosphere denitrification contributes to overall N_2O emissions from soil. We equipped rhizoboxes with O_2-sensitive planar optodes to simultaneously monitor root growth and rhizosphere/soil O_2 concentrations. We measured soil surface N_2O fluxes and linked them to root growth, soil moisture, and root/soil O_2 concentrations. Based on root growth and O_2 concentrations, we identified regions of interest (ROI) and sampled small soil volumes, which were analyzed for C, N, abundance of microbial denitrifiers (*nirK*, *nirS*) and N_2O reducers (*nosZI*, *nosZII*), and soil N_2O concentrations. Plant roots determined depth gradients of nutrients and denitrification gene abundances in the soil of the rhizoboxes with higher resource availability (NO_3^-, DOC) and lower soil moisture in the upper soil layers, which also had higher abundances of total bacteria, *nirK* and *nosZII*. We anticipate that these uppermost soil layers largely contributed to N_2O formation. For the first time we were able to show high *in-situ* N_2O concentrations with distinct depth profiles around roots, and O_2 and N availability controlling N_2O production at the process scale.

Introduction

Plant roots play an important role in regulating denitrification, the main process contributing to formation of the climate-relevant greenhouse gas nitrous oxide (N_2O) (Butterbach-Bahl *et al.*, 2013; Ciais *et al.*, 2013). Denitrification is the sequential reduction of nitrate (NO_3^-) to nitrite (NO_2^-), nitric oxide (NO), nitrous oxide (N_2O), and molecular nitrogen (N_2) by heterotrophic bacteria, fungi, and archaea (Zumft, 1997). Plant roots modify major controls of denitrification through altering soil moisture, O_2 content, the availability of its main substrates (NO_3^- and C_{org}), and root-associated microbial communities. While the rhizosphere is indicated to be a hotspot of denitrification, the extent of N_2O formation in the rhizosphere and its contribution to N_2O emissions from soils remain unclear.

Increased N_2O losses have been reported from planted compared to bare soils (Woldendorp, 1963; Vinther, 1984; Senbayram *et al.*, 2020; Yankelzon *et al.*, 2024b) and the promoting effect of plant growth on denitrification has been associated with higher C_{org} availability in the rhizosphere (Smith & Tiedje, 1979; Bakken, 1988; Philippot *et al.*, 2009). Plants translocate 20-30 % of assimilated C belowground and about 7-11 % of assimilated C enters the soil as rhizodeposition (Pausch & Kuzyakov, 2018). Higher C availability in the rhizosphere attracts soil microorganisms including bacteria, fungi, oomycetes, and archaea feeding on rhizodeposits making the rhizosphere a hotspot of microbial activity (Starkey, 1958; Philippot *et al.*, 2013). In addition to microbial respiration, root respiration largely contributes to O_2 consumption in soil with rates of around 20 mg O_2 m^{-1} root d^{-1} for maize roots (Ben-Noah & Friedman, 2018). Root and microbial respiration decrease O_2 availability, creating suitable conditions for denitrification (Bateman & Baggs, 2005; Hu *et al.*, 2015). Accordingly, abundance and composition of bacterial communities differ significantly between planted and unplanted soil, and between bulk soil and the rhizosphere (Chèneby *et al.*, 2004; Henry *et al.*, 2008; Philippot *et al.*, 2013). Studies show that denitrifiers are more abundant in the rhizosphere than the bulk soil of a range of different plant species (Knowles, 1982; Chèneby *et al.*, 2004; Ai *et al.*, 2020; Wang *et al.*, 2024). Accordingly, nitrate reduction and denitrification activities were higher in rhizosphere soil compared to bulk soil (Smith & Tiedje, 1979; Klemedtsson *et al.*, 1987; Bakken, 1988; Mahmood *et al.*, 1997; Hamonts *et al.*, 2013; Guyonnet *et al.*, 2017; Malique *et al.*, 2019; Zhao *et al.*, 2020).

Direct in-situ measurements of N_2O concentrations in the rhizosphere are lacking, yet crucial to understanding how roots control denitrification and N_2O formation. Further, it remains unknown to which extent rhizosphere denitrification contributes to overall N_2O emissions from soil and how microscale N_2O production relates to surface N_2O fluxes. Denitrification takes place in microbial hotspots – small soil volumes with faster process rates compared to the average soil conditions (=coldspots) (Groffman *et al.*, 2009; Kuzyakov & Blagodatskaya,

2015). Characterization of these N_2O hot and cold spots is needed to better understand the 'rhizosphere effect' and its significance for N_2O emissions.

This study aimed (I) to elucidate how plant roots control formation of N_2O hotspots in the rhizosphere, (II) to determine spatial distribution of N_2O production (hotspots) in relation to root growth and development, and (III) to characterize microbial N cycling in N_2O hotspots. We hypothesize that (I) root growth promotes microbial growth and respiration, increasing O_2 consumption at roots and in the rhizosphere. Accordingly, N_2O fluxes from soil increase with increasing root growth. (II) Increased microbial respiration from root exudation stimulates formation of anoxic microsites (N_2O hotspots) in close proximity of the roots. These N_2O hotspots are characterized by higher availability of C and N, and higher abundance of N reducing microorganisms compared to cold spots with low N_2O concentrations. To address these hypotheses, we equipped rhizoboxes with O_2-sensitive planar optodes to simultaneously monitor root growth and rhizosphere/soil O_2 concentrations. We further measured surface N_2O fluxes and linked them to root growth, soil moisture, and root/soil O_2 concentrations. Finaly, we defined regions of interest (ROI) related to root growth and O_2 concentrations, and analyzed them for C, N, abundance of microbial N reducers, and soil N_2O concentrations.

Material and Methods

Optode fabrication

Planar optodes are a non-invasive imaging technique based on reversible changes in luminescence properties of analyte-specific fluorophores enabling visualization and quantification of biochemical processes with an emphasis on capturing spatial and temporal heterogeneity (Blossfeld, 2013). The O_2 optodes were prepared as previously described by Merl & Koren (2020). 76.5 mg of the indicator dye PtTFPP (Platinum(II)-meso(2,3,4,5,6-pentafluoro)phenyl-porphyrin, Frontier Scientific, Newark, USA), 76.8 mg of the reference dye MY (Macrolex® fluorescence yellow 10GN, Lanxess, Köln, Germany), and 5 g Polystyrene (Sigma Aldrich, Burlington, USA) were dissolved in 50 g Toluene. This 'sensor cocktail' was knife-coated onto a PET foil (Optimont® 501, Bleher Folientechnik GmbH, Ditzingen-Heimerdingen, Germany) using a film applicator (BYK, Wesel, Germany) and a layer of ~10 µm was obtained after the toluene evaporated.

Soil

The soil was collected from a long-term experimental site in Rotthalmünster, Germany (N48°21′, E13°11′). It was characterized as Haplic Luvisol with a silty loamy texture (19 % clay, 71 % silt, 10 % sand), a pH ($CaCl_2$) of 6.74, with 0.13 % $CaCO_3$. The soil organic carbon

content was 1.21 %, total soil nitrogen was 0.14 %, and C:N ratio was 8.65. Soil was air-dried, sieved to 10 mm mesh size, and stored at 4 °C until the beginning of the experiment.

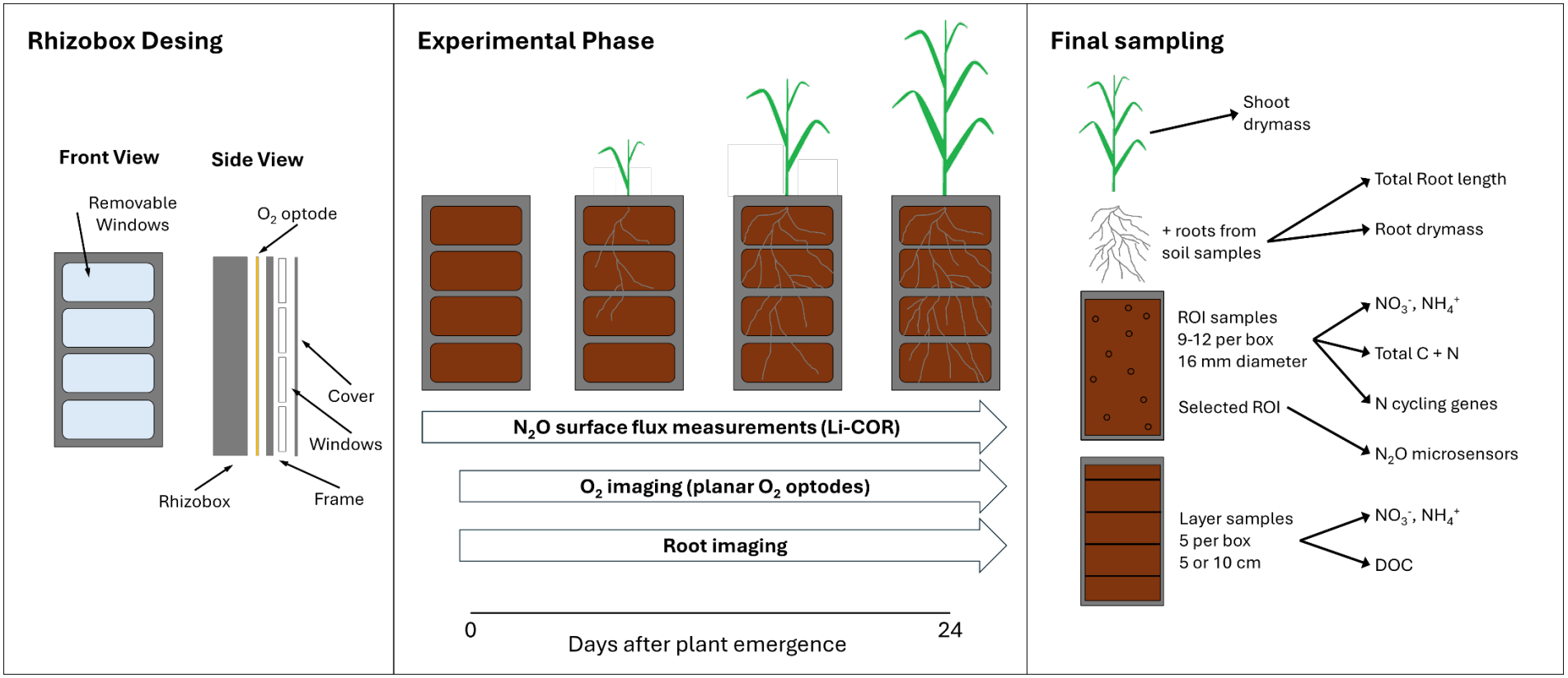

Figure 1: Schematic overview of rhizobox design, experimental phase, and final sampling of the experiment. The rhizobox covers consisted of an opaque frame with 4 removable window panels. To monitor O_2 concentrations in soil, an O_2-sensitive optode was attached to the frame before closing the rhizoboxes.

Experimental setup

The experiment was conducted in rhizoboxes with inner dimensions of 200 mm x 22 mm x 400 mm (width x depth x height). Each box had three holes (7 mm diameter) in the bottom part allowing for drainage. The inner sides were lined with a polyester wick (Breatex™ 150, Fibertex Nonwovens A/S, Aalborg, Denmark) facilitating rewetting and soil moisture distribution. The “window side” of the rhizoboxes consisted of an opaque frame and transparent, removable acrylic glass windows (Linatex A/S, Herlev, Denmark) (Figure 1). The O_2 optode was adhered onto the grid at the window side of the rhizoboxes with insulation tape. Rhizoboxes were closed using a rubber seal and C-clamps.

Dry soil was mixed with finely ground fertilizer (Pioner NPK Makro BLÅ, Azelis A/S, Kgs. Lyngby, Denmark) supplying 200 mg N kg^{-1}, 47 mg P kg^{-1}, 377 mg K kg^{-1}, 64 mg S kg^{-1}, and 49 mg Mg kg^{-1}. Seven rhizoboxes were filled with 2.2 kg of soil per box to a height of 38 cm, resulting in a bulk density of 1.3 g cm^{-3}. Soil was rewetted from the bottom over a period of 112 h and pre-incubated in a climate chamber (Weiss-Umwelttechnik GmbH, Gießen, Germany) for 10 days. One rhizobox was equipped with two FDR sensors (ECH2O 5TE, Decagon Devices, Pullman, USA) at 5-10 cm and 30-35 cm depth measuring volumetric soil water content and soil temperature. Rhizoboxes were weighed and watered every two-to-three days, always after N_2O flux measurements and O_2 imaging. Conditions in the climate chamber during preincubation and the experiment were as follows: 16 hours daylight with 300 µmol m^{-2} s^{-1} light intensity, 20 °C day temperature, 15 °C night temperature, 50 % relative humidity day, 60 % relative humidity night.

A Maize variety (*Zey mays* L. cv KWS Stabil) with higher rhizosheat mass (i.e., root-adhering soil) compared to other commercially available maize varieties (Koehler *et al.*, 2023) was chosen for this experiment. Seeds were pregerminated on wet paper for 3 days, and one germinated seed was planted into each box 10 days after rewetting the soil. Although maize seeds in all seven rhizoboxes were germinated and roots started growing in box 1-6, plants emerged in only two rhizoboxes (3 and 4) after 3-4 days. The remaining five rhizoboxes had to be replanted with small maize seedlings of the same variety.

N_2O surface flux analysis and calculations

Surface fluxes of N_2O emitted from soil were measured every two-to-three days using a N_2O/H_2O Trace Gas Analyzer (LI-7820, Li-COR, Lincoln, USA). Rhizoboxes were put into chambers consisting of an opaque bucket and a transparent chamber top. Chamber height was 50 cm, with a total volume of 36.2 L or adjusted to 150 cm (106.9 L) according to plant size. Chamber closing times were 4 and 10 minutes for small and large chambers, respectively. The temperature in the chamber was measured once at closing time and again before opening. The mean temperature was used for flux calculations. N_2O fluxes were

calculated using the R package *goFlux* v0.2.0 (Rheault *et al.*, 2024) and cumulative N_2O emissions were calculated using *agg.fluxes* from the R package *gasfluxes* v0.6-2 (Fuß, 2020).

O_2 and root imaging setup

The imaging of the O_2 optodes was conducted with a single-lens reflex (SLR) camera (EOS 1300D, Canon, Japan) equipped with an objective lens (EFS 18-55 mm Canon, Japan), and an orange 530 nm longpass filter (OG530 SCHOTT, 52 mm × 2 mm) with a plastic filter (#10 medium yellow, LEEfilters.com) attached in front of the long-pass filter to prevent autofluorescence of the longpass filter. For excitation of the optode, a blue LED (470 nm, r-s components, Copenhagen, Denmark) was used. The LED was controlled by a USB-controlled LED driver unit (imaging.fish-n-chips.de). The software look@RGB (imaging.fish-n-chips.de) was used to gather the images and to control the camera and LED. Calibration of the O_2 optode was done as described in detail by (Merl & Koren, 2020). O_2 imaging was conducted in two-to-three-day intervals, always on the same days as surface N_2O flux measurements.

Image processing and analysis was done using the software ImageJ (imagej.nih.gov/ij/) using a ratiometric approach (Larsen *et al.*, 2011; Merl & Koren, 2020). For the false-color images displaying O_2 concentration in % air saturation, the color palette *batlowK* (Scientific Color Maps v8.0.1, (Crameri, 2018) was used. We calculated the anoxic area of the rhizobox window as the proportion of the image area with an O_2 concentration < 10 % air saturation (28.4 µmol O_2/L) which is in the range of conditions promoting denitrification (Nakajima *et al.*, 1984; Bonin *et al.*, 1989) similar to previous studies (Zhu *et al.*, 2015; Keiluweit *et al.*, 2018).

Prior to O_2 imaging, a photo of the rhizoboxes was taken with 'normal light conditions' to monitor root growth on the rhizobox window side. These root images were analyzed with RootPainter (Smith *et al.*, 2022) to segment roots from the soil background. A model trained with randomly selected images was used to segment roots on all the images. Next, root length and root area were estimated from skeletonized images with RhizoVisionExplorer (Seethepalli *et al.*, 2021). For image pre-processing, we used a thresholding level of 200, removed non-root objects that were smaller than 1 mm, an edge smoothing threshold of 2, and a pruning threshold of 5.

N_2O microsensor measurements

We used needle-shaped clark-type N_2O microsensors that are based on an indium cathode in organic electrolyte, and an O_2-removing compartment measuring N_2O partial pressures (Pa) in both gas and liquid (Andersen *et al.*, 2001; Revsbech, 2021). Sensors were made inhouse, similar to those commercially available from Unisense (Unisense A/S, Aarhus, Denmark). The software SensorTrace Pro (Unisense A/S, Aarhus, Denmark) was used to introduce the sensor into the soil by a computer-controlled micromanipulator and to record the sensor signals. Calibration of the N_2O microsensors was performed in N_2O-free water by addition of an N_2O-

Standard (27 mM N_2O). All microsensors displayed a linear response curve during calibrations.

For N_2O microsensor measurements, small holes (2 x 2 mm) were cut into the optode foil and N_2O depth profiles (0- 5 mm) were measured in 500 µm steps. N_2O microsensor measurements were conducted in rhizobox 3 on day 7 and 15 after plant emergence. At the end of the experiment, 14 regions of interest (ROI) for N_2O microsensor measurements were chosen based on root development and O_2 concentration.

Harvest and soil sampling

The two rhizoboxes (Nr. 3 and 4), with initial seeds growing normally, were harvested 39 and 37 days after rewetting, corresponding to 25 and 21 days of plant growth, respectively. Rhizoboxes 1, 2, 5, 6, 7 with replanted seedlings were harvested 53, 49, 52, 50, and 52 days after rewetting, corresponding to 25, 21, 24, 22, and 24 days of plant growth. Due to the large workload of sampling and processing samples, it was not possible to sample all rhizoboxes on the same day. No physiological changes were observed between 21 and 25 days of plant growth. Shoots were cut above the surface and dried at 60 °C to determine shoot dry mass. Crown roots were added to the root samples.

In each rhizobox, regions of interest (ROI) were defined based on root development and O_2 concentration. Soil from ROI was sampled from the window side of the rhizoboxes with small aluminum cylinders (16 mm inner diameter, 10 mm depth) (UGT Umwelt-Geräte-Technik GmbH, Müncheberg, Germany) and the roots were carefully separated from the soil. The soil was then homogenized and divided into three subsamples: ~1 g soil (dry-weight-equivalent) was frozen in Eppendorf tubes (at – 20 °C for analysis of bacterial functional genes, ~1 g soil (dry-weight-equivalent) was stored in 10 ml centrifuge tubes at 4°C for analysis of mineral N, and the remaining soil (ca. 1-1.2 g) was dried at 105 °C to determine soil water content and total C and N content.

Additional soil samples were taken from rhizoboxes in 5 depths: 0-5 cm, 5-10 cm, 10-20 cm, 20-30 cm, 30-38 cm using a cork borer as auger (inner diameter 2 cm). For each depth layer, eight samples were taken and homogenized into one composite sample, after careful removal of the roots. Each composite sample was then divided into three subsamples: ~50 g soil (dry-weight-equivalent) was stored at 4°C for analysis of mineral N, ~10 g soil (dry-weight-equivalent) was stored at 4°C for analysis of water-extractable C_{org} (WEOC), and ~ 5 g soil (dry-weight-equivalent) were dried at 105° C to determine soil water content.

Roots were washed from the remaining soil and stored in 30 % ethanol at 4°C.

Root scanning and analysis

Roots were scanned on a flatbed scanner (Epson, Suwa, Japan) and the software RhizoVisionExplorer (Seethepalli *et al.*, 2021) was used to extract total root length and total

232 root volume from the scanned images. For image pre-processing, we used a thresholding
233 level of 200, removed non-root objects that were smaller than 0.1 px, an edge smoothing
234 threshold of 2, and a pruning threshold of 5. Root diameter classes were classified as <1mm,
235 1-2 mm, and >2 mm. Total root dry weight was determined by drying roots at 105 °C. We refer
236 to root length at the rhizobox window estimated with root imaging as *planar root length* and
237 root length at the final harvest measured with root scanning as *total root length* (Wacker *et al.*,
238 2024).

239 **Soil analysis**

240 Soil mineral N was extracted by shaking the subsample with 1 *M* KCl (ratio 1:5 w:v) on an
241 overhead shaker with 40 rpm for 60 min, filtered (Whatman Grade 42 for depth layer soil
242 samples, 0.8 µm CA syringe filters for ROI samples) and analyzed colorimetrically on a
243 continuous flow analyzer (AA3, Seal Analytical, Norderstedt, Germany). WEOC was extracted
244 by thoroughly shaking soil with ultrapure water (ratio 1:2 w:v) for 60 s, filtered through 0.45 µm
245 PES syringe filters, and analyzed on an elemental analyzer (multi N/C 2100 S, Analytik Jena,
246 Jena, Germany). Total C and N content in ROI samples was analyzed on an elemental
247 analyzer (Vario EL III, Elementar, Langenseibold, Germany).

248 **DNA extraction and quantitative PCR**

249 DNA was extracted from 400 mg of freeze-dried soil for each sample using the NucleoSpin
250 Soil kit (Macherey-Nagel, Düren, Germany), following the manufacturer's instructions. DNA
251 quality was checked using a NanoDrop (Thermo Fisher Scientific, Waltham, MA, USA), before
252 quantification on a Qubit fluorimeter using the Broad Range double stranded DNA kit (Thermo
253 Fisher Scientific). The abundance of total archaea and bacteria (16S rRNA gene), denitrifiers
254 (*nirK* and *nirS*) and N_2O reducers (*nosZ*I and *nosZ*II) were determined using real-time
255 quantitative PCR (qPCR) using specific primers for each gene. The qPCR reactions were
256 performed in two independent runs in a reaction volume of 15 µL containing iQ™ SYBR Green
257 Supermix (Bio-Rad, Hercules, CA, USA), 0.1 % bovine serum albumin (New England Biolabs,
258 Ipswich, MA, USA), primers and 2 ng of template DNA on a CFX Connect Real-Time System
259 (Bio-Rad). Primers, qPCR conditions, and amplification efficiencies are presented in
260 Supplementary Table S1. Standard curves were generated by serial dilutions of linearized
261 plasmids containing a fragment of the specific gene. The amplifications were validated by
262 melting curve analyses and agarose gel electrophoreses. Potential inhibition of PCR reactions
263 was initially checked by amplifying a known amount of the pGEM-T plasmid (Promega,
264 Madison, WI, USA) with the plasmid specific M13F/M13R primer set (Supplementary Table
265 S1) and 2 ng of DNA template or non-template controls for each sample. No inhibition was
266 detected with the amount of DNA used.

Calculations and statistics

All calculations and statistics were carried out using the statistical software R v4.3.3 (R Core Team, 2024). Simple linear regressions were applied to identify relationships between soil moisture, planar root length, or anoxic soil area. Similarly, we applied simple linear regression models to analyze relationships between soil N_2O concentrations, O_2 concentrations, N availability, and abundance of N cycling genes in ROI at the end of the experiment. To identify the factors driving N_2O fluxes, we applied linear mixed effect models (lme) using the lme function from the package nlme v3.1-131 (Pinheiro *et al.*, 2017). We tested models for the experimental period with and without plant growth, respectively, as well as for the whole experimental period. To account for repeated measurements, replicates were set as random effect. Models were compared using maximum likelihood (ML), selected using AIC (Akaike's information criterion), and fitted using restricted maximum likelihood (REML). Pseudo-R^2 for lme was calculated using r.squaredGLMM from the package MuMIn v1.42.1 (Barton, 2018).

Results

Plant and root growth

Root development followed the same pattern in all rhizoboxes. Planar root length increased slowly during the first week after emergence, then increased almost linearly until harvest (Fig. 2 a). Total root length at harvest ranged between 114 and 239 m, root dry weight ranged between 0.61 g and 2.0 g, and root dry weight was positively correlated with total root length (R^2=0.83, $p < 0.01$). Maize shoot dry weight at harvest ranged between 3.0 g and 7.1 g, and root:shoot ratio ranged between 0.22 and 0.31 (Supplementary Table S2). Shoot N content ranged between 2.8 and 4.0 % and shoot N uptake ranged between 98.0 and 198.7 mg N.

Soil Moisture

After rewetting, soil moisture ranged between 84 and 89 % WFPS (Supplementary Fig S1) and was kept at 65-70 % WFPS during plant growth, providing favorable conditions for anaerobic processes such as denitrification (Fig. 2b). Soil moisture sensors showed that soil moisture was very stable in the 30-35 cm layer and fluctuated most in the top 5-10 cm layer (Supplementary Figure S2).

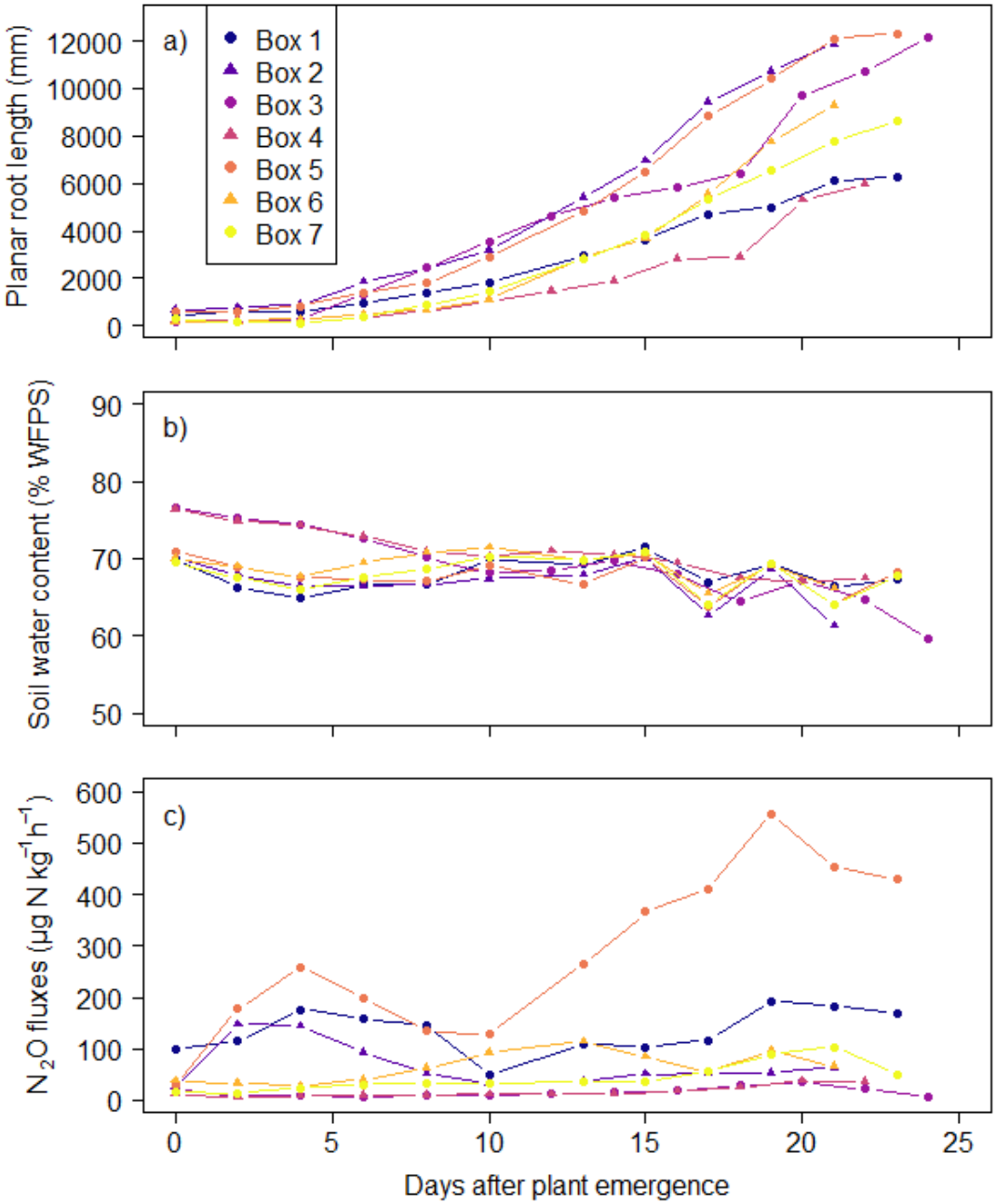

Figure 2: (a) Planar root length (mm), (b) soil water content (% water-filled pore space), and (c) N_2O fluxes (µg N_2O-N kg^{-1} h^{-1}) for each individual rhizobox.

N_2O fluxes and cumulative emissions

N_2O fluxes measured from the rhizoboxes showed large variations between treatments (Fig. 2c, Supplementary Fig. S1). During the acclimation phase, N_2O fluxes were comparable in all rhizoboxes and decreased for the first two weeks after rewetting. In the rhizoboxes that had to be replanted, N_2O fluxes remained relatively stable until plant emergence (Supplementary Fig S1). In rhizoboxes 1, 2, and 5, N_2O fluxes increased directly after plant emergence, in rhizobox 6, N_2O fluxes increased slightly a week after plant emergence, and N_2O fluxes from rhizoboxes 1, 5, and 7 increased towards the end of the experiment (Fig. 2c). N_2O fluxes from

box 1 were higher than all other rhizoboxes before plant emergence (Supplementary Fig. S1), and highest from rhizobox 5 after plant emergence (Fig. 2c).

Cumulative N_2O emissions during the planted phase ranged from 8.5 N_2O-N kg^{-1} to 157.5 and (Supplementary Fig. S3).

Soil O_2 concentrations and anoxic soil fraction

O_2 imaging started 10 days after rewetting in the rhizoboxes, and most of the optode-soil interface was anoxic at this time (Figure 3, Supplementary Figure S4 and S5). Overall, O_2 concentrations increased over time in all depths, although watering also led to formation of anoxic conditions in the upper soil layers without root growth (Figure 3). In the deeper soil layers, the rhizobox window area covered with the O_2-sensitive planar optode showed almost completely anoxic conditions throughout the experiment. During plant growth, the anoxic fraction decreased in all layers in all rhizoboxes as the soil became increasingly more oxic. O_2 concentrations rapidly increased in the topmost soil layer where more than 90 % of the window area was oxic 24 days after plant emergence. O_2 concentrations in the depths below followed similar patterns, with a time delay. With increasing root growth, larger areas became oxic, but in the direct vicinity of roots, O_2 concentrations were lower compared to surrounding bulk soil.

Interactions between root growth, soil moisture, soil profile O_2 concentrations, and surface N_2O fluxes

Soil water content and mean anoxic fraction were both negatively correlated with root length (R^2=0.27 and 0.85, respectively, $p < 0.0001$), while the anoxic fraction was positively correlated with soil water content (R^2=0.42, $p < 0.0001$) (Table 1, Supplementary Figure S6). Linear regressions between surface N_2O fluxes and either soil water content, root length, or anoxic fraction yielded only weak relationships (Table 1, Supplementary Figure S6).

The best model explaining surface N_2O fluxes included an interaction between soil water content and anoxic fraction as fixed factors and the rhizobox as random factor ($p < 0.01$). At a high anoxic fraction, $\ln(N_2O)$ was negatively correlated with soil water content, while $\ln(N_2O)$ was positively correlated with soil water content for low anoxic fractions pointing towards interactive effects of soil water content and anoxia on N_2O formation and reduction. The conditional R^2 of the full model was 0.86, while the marginal R^2 of the model with only the fixed effect (i.e., without the random factor) was 0.09 highlighting the large differences between treatments (Table 1, Supplementary Figure S7). Results of regression analyses for the dataset covering the whole experimental period can be found in the Supplementary Table S3.

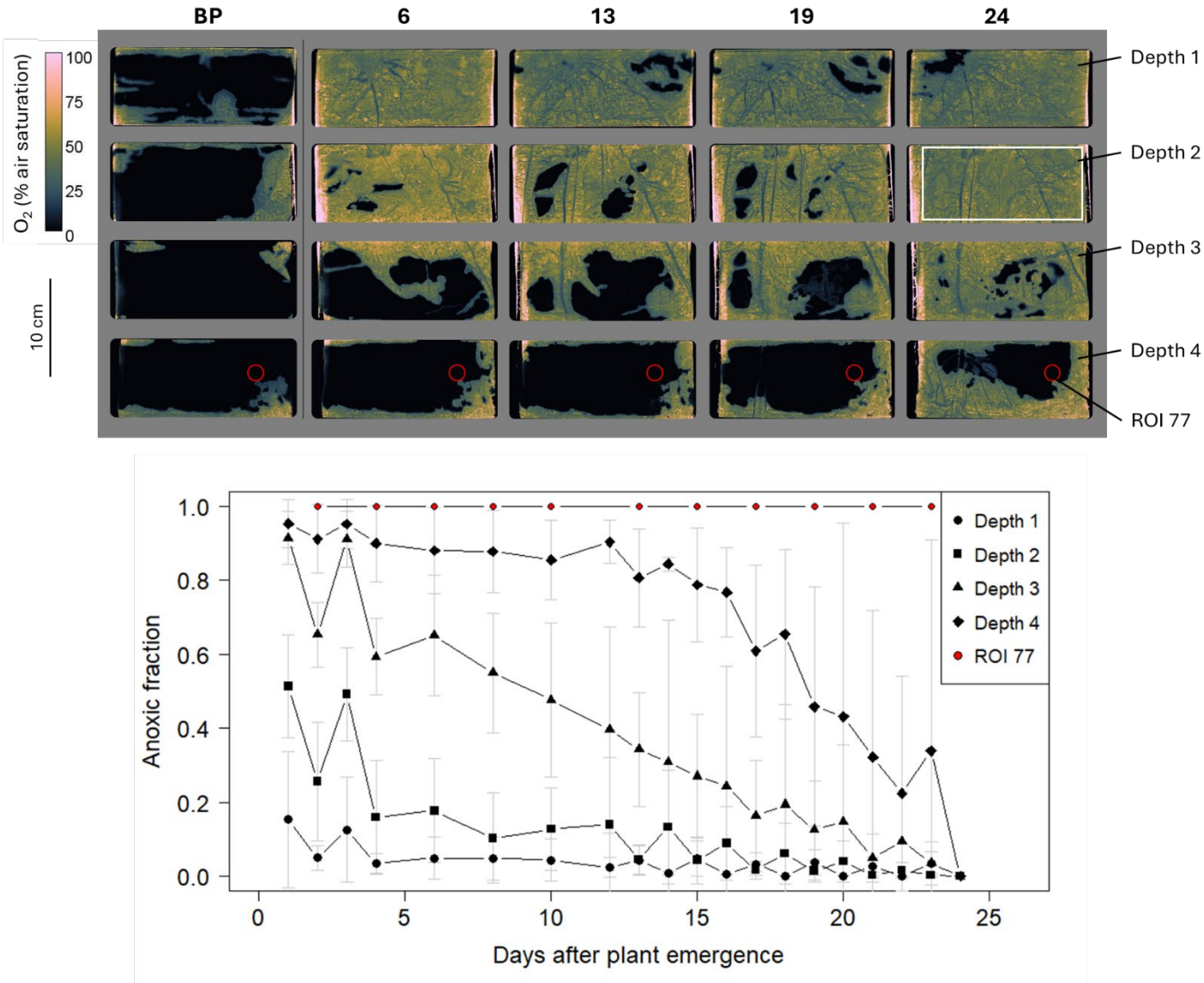

Figure 3: Top: False color images of the O_2 concentrations in Rhizobox 1 before plant emergence (BP) and on Day 6, 13, 19, and 24 after plant emergence measured with planar O_2 optodes. The four 'windows' of the rhizobox correspond to the four depths. The white rectangle is exemplary for the area used to calculate the anoxic fraction of each depth. Lighter areas outside the white rectangle are artifacts at the edges of the optode and were not included in calculations. The red circle represents ROI 77. Bottom: Fraction of anoxic area (< 10% O_2 air saturation = 2.1 % O_2). Different symbols represent the four depths in the rhizobox and ROI 77. Mean ± standard deviation for n=7.

Table 1: Results of regression analyses (coefficients of determination (Adjusted R^2), *p*-values, and sample size *n*) of the relationship between soil water content, root length, anoxic surface fraction, and N_2O surface fluxes (ln transformed).

Model	*n*	R^2	*p*-value
Simple linear regressions			
Soil water content ~ Root length	76	0.2738	7.42×10^{-07}
Anoxic fraction ~ Soil water content	76	0.4247	1.099×10^{-10}
Anoxic fraction ~ Root length	76	0.8482	$< 2.2 \times 10^{-16}$
$\ln(N_2O)$ ~ Root length	76	0.06972	0.01263
$\ln(N_2O)$ ~ Soil water content	76	0.1058	0.002411
$\ln(N_2O)$ ~ Anoxic fraction	76	0.115	0.001593
Linear mixed effect model			
$\ln(N_2O)$ ~ Soil water content * Anoxic Fraction Random effect: Rhizobox Nr (replicate)	76	0.857 (cond.)* 0.091 (marg.)*	0.0097

*For the linear mixed effect model (lme), the conditional R^2 is the variance explained by the entire model, including both fixed and random effects, while the marginal R^2 represents only the variance explained by the fixed effects.

Soil analyses (total CN, mineral N, WEOC)

Soil analyses showed similar depth patterns for analysis of soil layers and ROI (Figure 4). Soil NO_3^- content decreased with depth, from 320-1299 mg N kg^{-1} in the upper 5 cm to 1.7-502 mg N kg^{-1} in the 5-10 cm layer to 0.04-123 mg N kg^{-1} below 10 cm (Figure 4 a). Soil NH_4^+ contents were much lower compared to NO_3^- content. NH_4^+ contents were lowest in the 5-20 cm layers and ranged between 0 and 45 mg N kg^{-1} in the others (Figure 4b). Total soil N in ROI ranged between 0.09 and 0.26 % without clear differences in different depths (Supplementary Figure S8). Total soil C in ROI mostly ranged between 1.11 and 1.25 % which was similar to the initial soil C_{org} content (1.21 %). From 77 measured ROI, eight ROI had higher total C contents between 1.5 and 2.3 % which likely included small pieces of roots or $CaCO_3$. DOC content ranged between 24.5 and 188. 7 mg C kg^{-1} with highest values in 0-5 cm layers (Figure 4c).

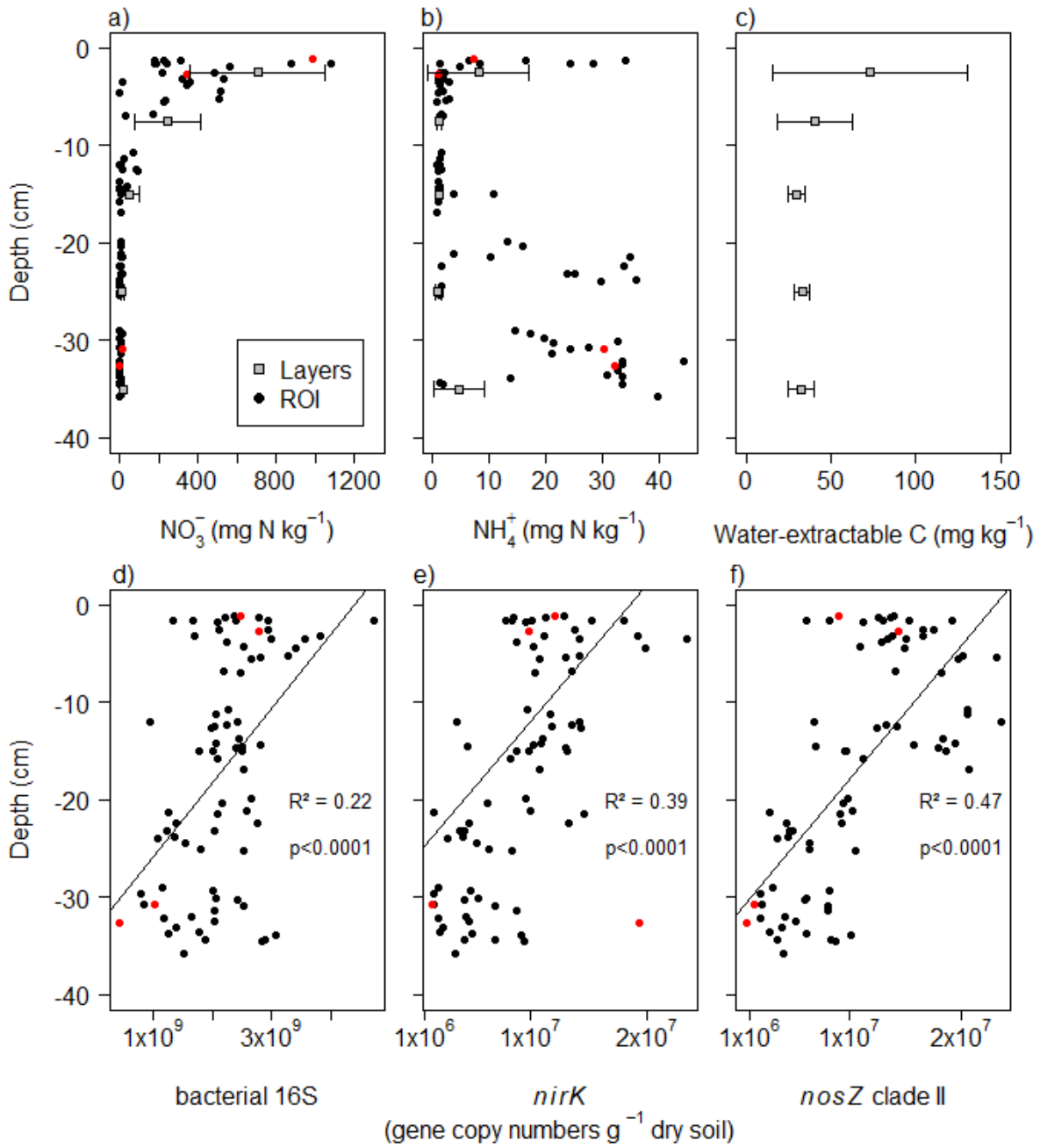

Figure 4: Depth distribution of (a) NO_3^-, (b) NH_4^+, and (c) DOC content in soil layers and ROI, and (d-f) depth distribution of gene abundances in ROI. Each black point represents one ROI, while grey squares represent mean values ± standard deviation for different soil layers (n=7). Red circles represent ROI Nr. 1, 6, 45, and 77. For gene abundances, regression lines, adjusted R^2, and *p*-values of simple linear regressions with depth are depicted.

Functional genes involved in N cycling

Abundance of 16S rRNA genes, a proxy for total archaea and bacteria, decreased with increasing sampling depth (R^2=0.22, $p < 0.0001$, Figure 4d, Table 2). Similarly, abundance of *nirK* and *nosZ* clade II genes decreased with increasing sampling depth (R^2=0.39 and 0.47, respectively, $p < 0.0001$). For *nirS* and *nosZ* clade I, only very weak correlations with sampling depth were found (Table 2). Except for *nirS*, gene abundances were negatively correlated with

soil NH_4^+ concentrations (Supplementary Table S4). However, NH_4^+ concentrations were also negatively correlated with soil depth. The ratio of denitrifiers (*nirK* + *nirS*) to N_2O reducers (*nosZ*I + *nosZ*II) increased with increasing NO_3^- content in ROI (R^2=0.2, $p < 0.0001$).

Table 2: Results of simple linear regression analyses (coefficients of determination (Adjusted R^2), *p*-values, and sample size *n*) of the relationship between N_2O, O_2, N concentrations, root growth, soil depth, and abundance of nitrogen cycling genes in ROI. Significant relationships ($p < 0.05$) are highlighted in bold.

Model	*n*	R^2	*p*-value
Root dry weight ~ total root length	**7**	**0.8303**	**0.002693**
Soil water content ~ total root length	**7**	**0.8899**	**0.0008959**
NO_3^- in 0-5 cm depth ~ Plant N uptake	7	0	0.9172
NO_3^- in 0-5 cm depth ~ Days of experiment	**7**	**0.8647**	**0.001511**
Total cumulative N_2O ~ NO_3^- in 0-5 cm depth	**7**	**0.484**	**0.04977**
Total cumulative N_2O ~ Days of experiment	7	0.3337	0.1018
Planted cumulative N_2O ~ Planted days	7	0.1891	0.1821
Planted cumulative N_2O ~ total root length	7	0	0.6273
Planted cumulative N_2O ~ Plant N uptake	7	0	0.6797
Min. N_2O ~ O_2 max	**14**	**0.5304**	**0.001893**
Max. N_2O ~ N concentration	**14**	**0.5227**	**0.002097**
16S ~ Depth	**77**	**0.2193**	**1.04×10^{-05}**
***nirK* ~ Depth**	**77**	**0.3882**	**8.65×10^{-10}**
nirS ~ Depth	77	0.04388	0.03745
nosZI ~ Depth	77	0.07119	0.01085
***nosZII* ~ Depth**	**77**	**0.4691**	**3.891×10^{-12}**
NH_4^+ ~ Depth	**77**	**0.3325**	**2.436×10^{-08}**
nirK ~ root age	**77**	**0.2431**	**3.127×10^{-06}**
***nosZII* ~ root age**	**77**	**0.1822**	**6.433×10^{-05}**
(*nirK*+*nirS*) / (*nosZI*+*nosZII*) ~ NO_3^-	**76**	**0.2**	**3.045×10^{-05}**

N_2O microsensor profiles in ROI and their relationship with influencing parameters

N_2O concentrations measured with N_2O microsensors in ROI at the end of the experiment showed very high variability in N_2O concentrations (Figure 5, Supplementary Figure S9). N_2O

concentrations ranged between 0 and 100 µmol N_2O L^{-1} with highest N_2O concentrations measured in ROI 1 close to the shoot and its crown roots in 1.1 cm depth and second highest measured in ROI 77 around a small root at the bottom of the rhizobox at 30.8 cm depth. N_2O depth profiles measured during the experiment are displayed in Supplementary Figure S10. For most ROI, changes in N_2O concentration within the same measurement profile were in the range of a few µmol (Supplementary Figure S9). There were exceptions, as ROI 1 where one N_2O profile increased from 20 to 100 µmol L^{-1} and ROI 77 where N_2O concentrations increased from 0 to 40-60 µmol L^{-1} in 2-5 mm depth (Figure 5). Minimum N_2O concentrations in 500 µm depth (i.e, in direct proximity to the optode) were negatively correlated with maximum O_2 concentration (R^2=0.53, $p < 0.01$, Table 2, Supplementary Figure S11), while maximum N_2O concentrations in 500 µm depth were positively correlated with total N availability in all ROI (R^2=0.52, $p < 0.01$, Table 2, Supplementary Figure S11).

ROI Nr. 45
No root
Depth = 2.7 cm

ROI Nr. 6
Root age = 7 days
Depth = 32.7 cm

ROI Nr. 77
Root age = 3 days
Depth = 30.8

ROI Nr. 1
Root age = 17 days
Depth = 1.1 cm

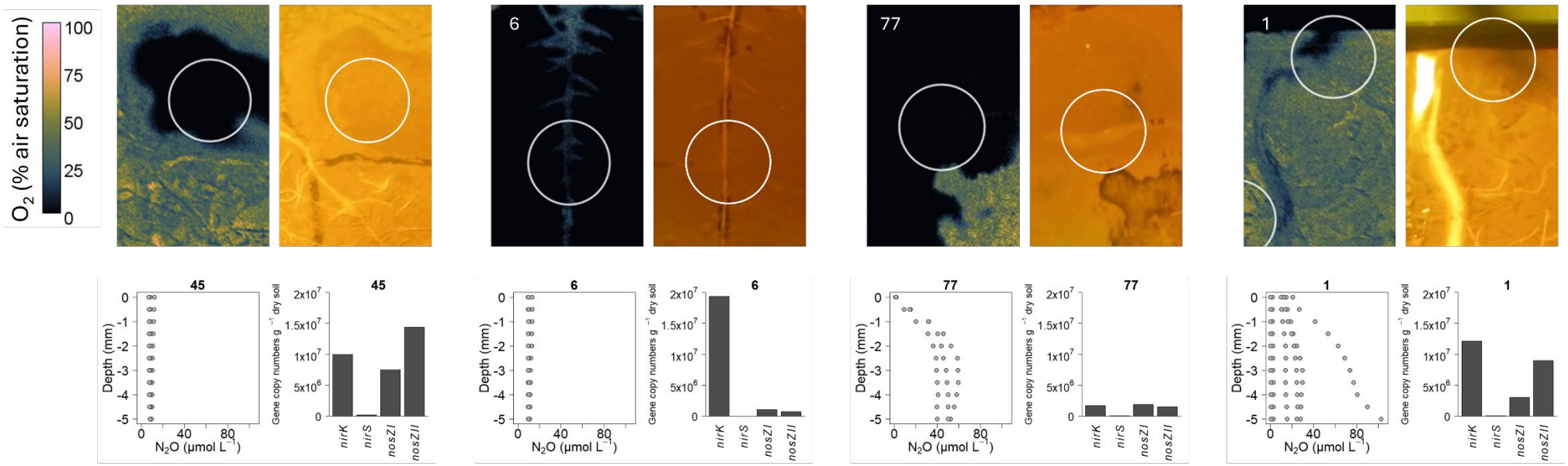

NO_3^- = 345 mg kg^{-1}
NH_4^+ = 1.03 mg kg^{-1}

NO_3^- = 0.37 mg kg^{-1}
NH_4^+ = 32.11 mg kg^{-1}

NO_3^- = 12.02 mg kg^{-1}
NH_4^+ = 30.19 mg kg^{-1}

NO_3^- = 990 mg kg^{-1}
NH_4^+ = 7.27 mg kg^{-1}

Figure 5: Characterization of four exemplary ROI at the end of the experiment. False-color image showing O_2 concentration, photo showing root development, N_2O microsensor depth profiles (µmol N_2O), barplot showing gene abundances (gene copy numbers g^{-1} dry soil), and mineral N content (mg N kg^{-1}). ROI diameter = 16 mm. Root age refers to the days of root growth in the respective ROI.

Discussion

Microsite N_2O formation depended on root growth, O_2 and N availability

N_2O microsensor measurements showed very high spatial heterogeneity of N_2O formation in soil. Minimum N_2O concentrations were higher in ROI with lower O_2 concentrations confirming that O_2 availability was a major control of denitrification at the microsite scale. Oxygen concentration is one of the most important controls of denitrification as it determines when microorganisms switch to anaerobic respiration (Groffman *et al.*, 1988; Schlüter *et al.*, 2024). This, however, does not ascertain that denitrification will occur, as nitrate can be limiting (Smith & Tiedje, 1979; Hojberg *et al.*, 1994; Schlüter *et al.*, 2024), which has been documented in relation to plant growth with rapid N uptake (von Rheinbaben & Trolldenier, 1984; Haider *et al.*, 1985; Rummel *et al.*, 2021). Accordingly, we found higher N_2O concentrations in ROI with higher total N availability indicating that, under O_2 limiting conditions, N availability is crucial to determine the magnitude of N_2O emissions. ROI with the highest N_2O concentrations were in the direct vicinity of roots (i.e., ROI Nr. 1, 77). In contrast, ROI 45 was characterized by high NO_3^- content and anoxic conditions, but no roots, and only low N_2O concentrations confirming the importance of roots on formation of N_2O hotspots through C exudation, root and rhizosphere microbial respiration, verifying our second hypothesis. Although functional gene abundances and N_2O concentrations were not significantly correlated in ROI, we found a positive relationship between the (*nirK*+*nirS*)/(*nosZI*+*nosZII*) ratio and NO_3^- availability indicating higher relative genetic potential for N_2O reduction at lower soil NO_3^- content. This relationship was driven by the abundance of *nosZ* clade II nitrous oxide reducers, in line with previous reports (Xu *et al.*, 2020; Jones *et al.*, 2022).

Roots determined biotic and abiotic gradients in soil

Plant and root growth affected soil moisture, anoxic soil fraction, and distribution of nutrients controlling the abundance of microorganisms. Root growth determined soil moisture through root water uptake as demonstrated by significant negative correlations between soil water content and planar root length throughout the experiment and between soil water content and total root length at final harvest. Further, soil moisture sensors showed that soil moisture was constant at the bottom of the rhizoboxes, while fluctuating more in the upper soil layer with higher root density. Using planar optodes, we were able to show increasing O_2 concentrations with increasing plant and root growth. Especially, roots growing into deeper soil layers led to increasing O_2 concentrations at the optode-soil interface. We anticipate a combination of several explanations: (1) plant roots can increase the diffusion of O_2 through the soil (Jensen & Kirkham, 1963), (2) maize roots form aerenchyma under O_2-limited conditions (≤ 3% O_2 ≈ 14.3 % O_2 air saturation (Gunawardena *et al.*, 2001) facilitating transport of O_2 into anoxic soil

438 layers, (3) and roots may have 'pushed' the optode away from the soil surface in some spots
439 creating air-filled cavities between the optode and the soil (Merl *et al.*, 2023). Although roots
440 generally increased aeration and O_2 concentrations in soil, roots were always characterized
441 by lower O_2 concentrations compared to the surrounding soil confirming our first hypothesis.
442 Most of the added NO_3^- fertilizer was recovered in the upper 10 cm of the rhizoboxes likely
443 due to a combination of initial rewetting the soil in the rhizoboxes from the bottom and
444 evaporation on the soil surface causing a constant upward movement of soil water,
445 transporting NO_3^- to the upper soil layer throughout the experiment. Root growth increased
446 availability of organic C through rhizodeposition leading to higher DOC concentrations in upper
447 soil layers with higher root density. Although root exudation per root surface area decreases
448 with growth/age, total exuded C rates increase with increasing root growth (Santangeli *et al.*,
449 2024). Especially, maize crown/brace roots can exude large quantities of mucilage containing
450 high amounts of sugars (Werner *et al.*, 2022) contributing to high availability of DOC in the
451 uppermost soil layers. Higher availability of DOC and NO_3^- in upper soil layers promoted
452 microbial growth as indicated by decreasing abundances of 16S rRNA, *nirK* and *nosZII* genes
453 with soil depth. Abundances of *nirK* and *nosZII* genes also increased with increasing root age
454 confirming the influence of root growth on microbial denitrifiers. Abundances of *nirS* and *nosZI*
455 were much lower compared to abundances of *nirK* and *nosZII*, respectively, and were not
456 affected by nutrient concentrations or root growth indicating niche differentiation between *nirK*-
457 and *nirS*-type denitrifiers and *nosZ* clade I and II nitrous oxide reducers, respectively (Jones
458 & Hallin, 2010; Achouak *et al.*, 2019; Wang *et al.*, 2024).

459 **Soil moisture and anoxic fraction controlled N_2O fluxes**

460 N_2O fluxes showed distinct patterns with initially high fluxes decreasing until about two weeks
461 after rewetting the soil, followed by a period with lower fluxes. Emergence of plants stimulated
462 N_2O production leading to clear increases in N_2O fluxes within a week following plant
463 emergence. However, correlations between N_2O fluxes and planar root length or cumulative
464 N_2O emissions and total root length at harvest did not yield significant relationships as we
465 would have expected. Nonetheless, our study confirmed intercorrelation of root growth and
466 N_2O formation as N_2O fluxes were controlled by an interaction of the anoxic fraction and soil
467 moisture, confirming interacting effects of root water uptake and anaerobicity on N_2O formation
468 and reduction. For low anoxic fractions, increasing soil moisture led to increasing N_2O fluxes,
469 while for high anoxic fractions higher soil moisture led to lower N_2O fluxes due to the reduction
470 of N_2O to N_2 (Davidson, 1991; Rohe *et al.*, 2021). In addition, differences between replicates
471 explained most of the variance in N_2O fluxes. Soil heterogeneity is known to strongly control
472 the formation of denitrifying N_2O hotspots causing very high variation within replicates of the
473 same treatment (Folorunso & Rolston, 1984; Christensen *et al.*, 1990; Schlüter *et al.*, 2024).

Plant and root growth further increased heterogeneity in soil but also differences between replicates.

The uppermost soil layers contributed largely to N_2O fluxes

We anticipated that some zones of the rhizoboxes were more likely to contribute to N_2O formation – the uppermost and the lowest soil layers. The upper 5 cm soil layer was characterized by very high NO_3^- concentrations (up to >1000 mg NO_3^--N kg^{-1}), highest concentrations of DOC, and highest abundances of denitrifying and N_2O reducing genes (*nirK* and *nosZII*). Although O_2 concentrations in the uppermost soil layer increased fast, small anoxic areas were identified with the O_2 optodes at the later/last measurement days. Furthermore, rewatering from the top kept soil continuously wet which (together with high NO_3^- and DOC) provided optimal conditions for denitrifiers as confirmed by microsensor measurements (ROI 1). Short distance to the soil surface facilitated N_2O diffusion to the surface and its loss to the atmosphere. Accordingly, cumulative N_2O emissions were positively correlated with soil NO_3^- content in the uppermost soil layer. In contrast, the bottom layer of the rhizoboxes had larger areas that remained anoxic throughout the experiment. NO_3^- concentrations in the bottom layer were low (15 mg NO_3^--N kg^{-1}, 200 µM NO_3^-), but sufficient to sustain denitrifying microorganisms (Palmer & Horn, 2015) as confirmed by N_2O microsensor profiles indicating substantial N_2O formation around a small root in ROI 77. Continuous high soil moisture and long diffusion pathways from the lower layers of the rhizobox to the soil surface likely promoted N_2O reduction to N_2, which has been reported for this particular soil (Malique *et al.*, 2019; Rummel *et al.*, 2021; Yankelzon *et al.*, 2024a).

Conclusions

We provide the first *in-situ* measurements of N_2O concentration profiles showing distinct patterns with highest N_2O concentrations around roots compared to bulk soil. Our study confirmed that O_2 and N availability control N_2O production at the process scale while emphasizing the importance of roots in shaping N_2O hotspots. Plant roots determined depth gradients in the soil of the rhizoboxes with higher DOC and lower soil moisture in the upper soil layers. Abundances of total bacteria, denitrifying *nirK* and N_2O reducing *nosZII* responded to resource availability with higher abundances in upper soil layers with high nutrient contents and more root growth. We argue that these uppermost soil layers largely contributed to N_2O formation and N_2O fluxes measured at the soil surface. Combining O_2 optode and root imaging proved to be a successful approach to monitor major controls of rhizosphere N cycling and N_2O formation at high spatial and temporal resolution. Carefully choosing ROIs allowed reducing the number of samples, while covering a broad range of soil conditions revealing

correlations between N_2O concentrations, substrate availability, and microbial gene abundances.

Acknowledgements

The authors would like to thank Lars Borregaard Pedersen for excellent technical support, Tomke S. Wacker, Frederik van der Bom, and Lorène Siegwart for support on root imaging, scanning, and analysis, Andrey Kalinichev and Fabian Steininger for help with optode calibration, Sabine Rautenberg and Claudia Kuntz for soil analyses, Franziska Eller for the climate chambers and LiCOR, and Per Lennart Ambus and Kristian Thorup-Kristensen for feedback on the experimental setup.

PSR was supported by a Novo Nordisk Fonden (NNF) Postdoctoral Fellowship (grant number NNF22OC0079335). MRR was supported by the Pioneer Center for Research in Sustainable Agricultural Futures (Land-CRAFT), DNRF grant number P2.

Competing interests

The authors declare no competing interests.

Author contributions

Conceptualization: PSR, CWM, KK; Investigation: PSR, MRR, AS; Data analysis (soil, root, N_2O): PSR; Data analysis (optodes): PSR, TM; Data analysis (qPCR): AS; Writing – original draft preparation: PSR; Writing – review and editing: MRR, AS, TM, SH, CWM, KK. All authors have read and agreed to the published version of the manuscript.

Data availability

The data that support the findings of this study will be made openly available at http://doi.org/10.5281/zenodo.15537545.

References

Achouak W, Abrouk D, Guyonnet J, Barakat M, Ortet P, Simon L, Lerondelle C, Heulin T, El Zahar Haichar F. **2019**. Plant hosts control microbial denitrification activity. *FEMS Microbiology Ecology* **95**: 1–13.

Ai C, Zhang M, Sun Y, Zhang L, Zeng L, Liu Y, Wang X, Chai Y, He P, Liang G, *et al.* 2020. Wheat rhizodeposition stimulates soil nitrous oxide emission and denitrifiers harboring the nosZ clade I gene. *Soil Biology and Biochemistry* **143**.

Andersen K, Kjar T, Revsbech NP. **2001**. An oxygen insensitive microsensor for nitrous oxide. *Sensors and Actuators, B: Chemical* **81**: 42–48.

Bakken LR. **1988**. Denitrification under different cultivated plants: effects of soil moisture tension, nitrate concentration, and photosynthetic activity. **6**: 271–278.

Barton K. **2018**. MuMIn: Multi-Model Inference.

Bateman EJ, Baggs EM. **2005**. Contributions of nitrification and denitrification to N2O emissions from soils at different water-filled pore space. *Biology and Fertility of Soils* **41**: 379–388.

Ben-Noah I, Friedman SP. **2018**. Review and Evaluation of Root Respiration and of Natural and Agricultural Processes of Soil Aeration. *Vadose Zone Journal* **17**: 170119.

Blossfeld S. **2013**. Light for the dark side of plant life: -Planar optodes visualizing rhizosphere processes. *Plant and Soil* **369**: 29–32.

Bonin P, Gilewicz M, Bertrand JC. **1989**. Effects of oxygen on each step of denitrification on Pseudomonas nautica. *Canadian Journal of Microbiology* **35**: 1061–1064.

Butterbach-Bahl K, Baggs EM, Dannenmann M, Kiese R, Zechmeister-Boltenstern S. **2013**. Nitrous oxide emissions from soils: how well do we understand the processes and their controls ? *Philosophical transactions of the Royal Society B* **368**: 1–13.

Chèneby D, Perrez S, Devroe C, Hallet S, Couton Y, Bizouard F, Iuretig G, Germon JC, Philippot L. **2004**. Denitrifying bacteria in bulk and maize-rhizospheric soil: diversity and N_2O-reducing abilities. *Canadian Journal of Microbiology* **50**: 469–474.

Christensen S, Groffman P, Mosier A, Zak DR. **1990**. Rhizosphere Denitrification; A Minor Process but Indicator of Decomposition Activity. In: Denitrification in Soil and Sediment. 199–211.

Ciais P, Sabine C, Bala G, Bopp L, Brovkin V, Canadell J, Chhabra A, DeFries R, Galloway J, Heimann M, *et al.* 2013. Carbon and Other Biogeochemical Cycles. In: Climate Change 2013: The Physical Science Basis. Contribution of Working Group I to the Fifth Assessment Report of the Intergovernmental Panel on Climate Change. 465–570.

Crameri F. **2018**. Scientific Colour Maps.

Davidson EA. **1991**. Fluxes of nitrous oxide and nitric oxide from terrestrial ecosystems. In: Rogers JE, Whitman WB, eds. Microbial Production and Consumption of Greenhouse Gases: Methane, Nitrogen Oxides and Halomethanes. Washington (DC): American Society for Microbiology, 219–235.

Folorunso OA, Rolston DE. **1984**. Spatial Variability of Field-Measured Denitrification Gas Fluxes. *Soil Science Society of America Journal* **48**: 1214–1219.

Fuß R. **2020**. gasfluxes: Greenhouse Gas Flux Calculation from Chamber Measurements.

Groffman PM, Butterbach-Bahl K, Fulweiler RW, Gold AJ, Morse JL, Stander EK, Tague C, Tonitto C, Vidon P. **2009**. Challenges to incorporating spatially and temporally explicit phenomena (hotspots and hot moments) in denitrification models. *Biogeochemistry* **93**: 49–77.

Groffman PM, Tiedje JM, Robertson GP, Christensen S. **1988**. Denitrification at different temporal and geographical scales: Proximal and distal controls. In: Wilson JR, ed. Advances in Nitrogen Cycling in Agricultural Ecosystems. 174–192.

Gunawardena AHLAN, Pearce DME, Jackson MB, Hawes CR, Evans DE. **2001**. Rapid changes in cell wall pectic polysaccharides are closely associated with early stages of aerenchyma formation, a spatially localized form of programmed cell death in roots of maize (Zea mays L.) promoted by ethylene. *Plant, Cell and Environment* **24**: 1369–1375.

Guyonnet JP, Vautrin F, Meiffren G, Labois C, Cantarel AAM, Michalet S, Comte G, Haichar F el Z. **2017**. The effects of plant nutritional strategy on soil microbial denitrification activity through rhizosphere primary metabolites. *FEMS Microbiology Ecology* **93**: 1–11.

Haider K, Mosier A, Heinemeyer O. **1985**. Phytotron Experiments to Evaluate the Effect of Growing Plants on Denitrification. *Soil Science Society of America Journal* **49**: 636–641.

Hamonts K, Clough TJ, Stewart A, Clinton PW, Richardson AE, Wakelin SA, O'Callaghan M, Condron LM. **2013**. Effect of nitrogen and waterlogging on denitrifier gene abundance, community structure and activity in the rhizosphere of wheat. *FEMS Microbiology Ecology* **83**: 568–584.

Henry S, Texier S, Hallet S, Bru D, Dambreville C, Chèneby D, Bizouard F, Germon JC, Philippot L. **2008**. Disentangling the rhizosphere effect on nitrate reducers and denitrifiers: Insight into the role of root exudates. *Environmental Microbiology* **10**: 3082–3092.

Hojberg O, Revsbech NP, Tiedje JM. **1994**. Denitrification in Soil Aggregates Analyzed with Microsensors for Nitrous Oxide and Oxygen. *Soil Science Society of America Journal* **58**: 1691–1698.

Hu HW, Chen D, He JZ. **2015**. Microbial regulation of terrestrial nitrous oxide formation: Understanding the biological pathways for prediction of emission rates. *FEMS Microbiology Reviews* **39**: 729–749.

Jensen CR, Kirkham D. **1963**. *Labeled Oxygen: Increased Diffusion Rate through Soil Containing Growing Corn Roots*.

Jones CM, Hallin S. **2010**. Ecological and evolutionary factors underlying global and local assembly of denitrifier communities. *ISME Journal* **4**: 633–641.

Jones CM, Putz M, Tiemann M, Hallin S. **2022**. Reactive nitrogen restructures and weakens microbial controls of soil N2O emissions. *Communications Biology* **5**.

Keiluweit M, Gee K, Denney A, Fendorf S. **2018**. Anoxic microsites in upland soils dominantly controlled by clay content. *Soil Biology and Biochemistry* **118**: 42–50.

Klemedtsson L, Svensson BH, Rosswall T. **1987**. Dinitrogen and nitrous oxide produced by denitrification and nitrification in soil with and without barley plants. *Plant and Soil* **99**: 303–319.

Knowles R. **1982**. Denitrification. *Microbiolagical Reviews* **46**: 43–70.

Koehler T, Schaum C, Tung S-Y, Steiner F, Tyborski N, Wild AJ, Akale A, Pausch J, Lueders T, Wolfrum S, *et al.* 2023. Above and belowground traits impacting transpiration decline during soil drying in 48 maize (Zea mays) genotypes. *Annals of Botany* **131**: 373–386.

Kuzyakov Y, Blagodatskaya EV. **2015**. Microbial hotspots and hot moments in soil: Concept & review. *Soil Biology and Biochemistry* **83**: 184–199.

Larsen M, Borisov SM, Grunwald B, Klimant I, Glud RN. **2011**. A simple and inexpensive high resolution color ratiometric planar optode imaging approach: application to oxygen and pH sensing. *Limnology and Oceanography: Methods* **9**: 348–360.

Mahmood T, Ali R, Malik KA, Shamsi SRA. **1997**. Denitrification with and without plant (Zea mays L.) under irrigated field conditions. *Biol Fert Soils* **24**: 323–328.

Malique F, Ke P, Boettcher J, Dannenmann M, Butterbach-Bahl K. **2019**. Plant and soil effects on denitrification potential in agricultural soils. *Plant and Soil* **439**: 459–474.

Merl T, Hu Y, Pedersen J, Zieger SE, Bornø ML, Tariq A, Sommer SG, Koren K. **2023**. Optical Chemical Sensors for Soil Analysis: Possibilities and Challenges of Visualizing NH3 Concentrations as well as pH and O2 Microscale Heterogeneity. *Environmental Science: Advances* **00**: 1–10.

Merl T, Koren K. **2020**. Visualizing NH3 emission and the local O2 and pH microenvironment of soil upon manure application using optical sensors. *Environment International* **144**: 106080.

Nakajima M, Hayamizu T, Nishimura H. **1984**. Effect of oxygen concentration on the rates of denitratification and denitrification in the sediments of an eutrophic lake. *Water Research* **18**: 335–338.

Palmer K, Horn MA. **2015**. Denitrification activity of a remarkably diverse fen denitrifier community in Finnish Lapland is N-oxide limited. *PLoS ONE* **10**.

Pausch J, Kuzyakov Y. **2018**. Carbon input by roots into the soil: Quantification of rhizodeposition from root to ecosystem scale. *Global Change Biology* **24**: 1–12.

Philippot L, Hallin S, Börjesson G, Baggs EM. **2009**. Biochemical cycling in the rhizosphere having an impact on global change. *Plant and Soil* **321**: 61–81.

Philippot L, Raaijmakers JM, Lemanceau P, Van Der Putten WH. **2013**. Going back to the roots: The microbial ecology of the rhizosphere. *Nature Reviews Microbiology* **11**: 789–799.

Pinheiro J, Bates D, DebRoy S, Sarkar D, R Core Team. **2017**. nlme: Linear and Nonlinear Mixed Effects Models.

R Core Team. **2024**. R: A Language and Environment for Statistical Computing.

Revsbech NP. **2021**. Simple sensors that work in diverse natural environments: The micro-Clark sensor and biosensor family. *Sensors and Actuators, B: Chemical* **329**: 129168.

Rheault K, Christiansen JR, Larsen KS. **2024**. goFlux: A user-friendly way to calculate GHG fluxes yourself, regardless of user experience. *Journal of Open Source Software* **9**: 6393.

von Rheinbaben W, Trolldenier G. **1984**. Influence of plant growth on denitrification in relation to soil moisture and potassium nutrition. *Zeitschrift für Pflanzenernärung und Bodenkunde* **147**: 730–738.

Rohe L, Apelt B, Vogel H-J, Well R, Wu G-M, Schlüter S. **2021**. Denitrification in soil as a function of oxygen availability at the microscale. *Biogeosciences* **18**: 1185–1201.

Rummel PS, Well R, Pfeiffer B, Dittert K, Floßmann S, Pausch J. **2021**. Nitrate uptake and carbon exudation – do plant roots stimulate or inhibit denitrification? *Plant and Soil* **459**: 217–233.

Santangeli M, Steininger-Mairinger T, Vetterlein D, Hann S, Oburger E. **2024**. Maize (Zea mays L.) root exudation profiles change in quality and quantity during plant development – A field study. *Plant Science* **338**.

Schlüter S, Lucas M, Grosz B, Ippisch O, Zawallich J, He H, Dechow R, Kraus D, Blagodatsky S, Senbayram M, *et al.* 2024. The anaerobic soil volume as a controlling factor of denitrification: a review. *Biology and Fertility of Soils*.

Seethepalli A, Dhakal K, Griffiths M, Guo H, Freschet GT, York LM. **2021**. RhizoVision Explorer: Open-source software for root image analysis and measurement standardization. *AoB PLANTS* **13**: 1–15.

Senbayram M, Well R, Shan J, Bol R, Burkart S, Jones DL, Wu D. **2020**. Rhizosphere processes in nitrate-rich barley soil tripled both N2O and N2 losses due to enhanced bacterial and fungal denitrification. *Plant and Soil* **448**: 509–522.

Smith AG, Han E, Petersen J, Olsen NAF, Giese C, Athmann M, Dresbøll DB, Thorup-Kristensen K. **2022**. R <scp>oot</scp> P <scp>ainter</scp> : deep learning segmentation of biological images with corrective annotation. *New Phytologist* **236**: 774–791.

Smith MS, Tiedje JM. **1979**. PHASES OF DENITRIFiCATION FOLLOWING OXYGEN DEPLETION IN SOIL. *Soil Biology and Biochemistry* **11**: 261–267.

Starkey RL. **1958**. INTERRELATIONS BETWEEN MICROORGANISMS AND PLANT ROOTS IN THE RHIZOSPHERE. *Bacteriological Reviews* **22**: 154–172.

Vinther FP. **1984**. Total denitrification and the ratio between N2O and N2 during the growth of spring barley. *Plant and Soil* **76**: 227–232.

Wacker TS, van der Bom F, Delory BM, Vetterlein D, Postma JA, Nagel KA, Schnepf A, Dresbøll DB. **2024**. Back to the roots: standardizing root length density terminology. *Plant and Soil*.

Wang J, Zhang Z, Liang F, Che Z, Wen Y, Zhang M, Jin W, Dong Z, Song H. **2024**. Decreased soil pH weakens the positive rhizosphere effect on denitrification capacity. *Pedosphere* **34**: 905–915.

Werner LM, Knott M, Diehl D, Ahmed MA, Banfield C, Dippold M, Vetterlein D, Wimmer MA. **2022**. Physico-chemical properties of maize (Zea mays L.) mucilage differ with the collection system and corresponding root type and developmental stage of the plant. *Plant and Soil* **478**: 103–117.

Woldendorp W. **1963**. The Influence of Living Plants on Denitrification. *Meded Landbouwhogeschool Wageningen* **63**: 1–100.

Xu X, Liu Y, Singh BP, Yang Q, Zhang Q, Wang H, Xia Z, Di H, Singh BK, Xu J, *et al.* 2020. *Nos*Z clade II rather than clade I determine *in situ* N2O emissions with different fertilizer types under simulated climate change and its legacy. *Soil Biology and Biochemistry* **150**: 107974.

Yankelzon I, Schilling L, Butterbach-Bahl K, Gasche R, Han J, Hartl L, Kepp J, Matson A, Ostler U, Scheer C, *et al.* 2024a. Lysimeter-based full fertilizer 15N balances corroborate direct dinitrogen emission measurements using the 15N gas flow method. *Biology and Fertility of Soils*.

Yankelzon I, Willibald G, Dannenmann M, Malique F, Ostler U, Scheer C, Butterbach-Bahl K. **2024b**. A new incubation system to simultaneously measure n2 as well as n2o and co2 fluxes from plant-soil mesocosms. *Biology and Fertility of Soils*.

Zhao S, Zhou J, Yuan D, Wang W, Zhou L, Pi Y, Zhu G. **2020**. NirS-type N2O-producers and nosZ II-type N2O-reducers determine the N2O emission potential in farmland rhizosphere soils. *Journal of Soils and Sediments* **20**: 461–471.

Zhu K, Bruun S, Larsen M, Glud RN, Jensen LS. **2015**. Heterogeneity of O2 dynamics in soil amended with animal manure and implications for greenhouse gas emissions. *Soil Biology and Biochemistry* **84**: 96–106.

Zumft WG. **1997**. Cell biology and molecular basis of denitrification. *Microbiology and Molecular Biology Reviews* **61**: 533–616.